https://doi.org/10.5194/egusphere-2026-6900
Preprint. Discussion started: 12 November 2026
© Author(s) 2026. CC BY 4.0 License.

Day-To-Day Variability of Nonmigrating Tides Derived from Sparse Meteor Radar Data

Jianyuan Wang[1,2], Wen Yi[3,4,*], Xianghui Xue[3,4,5,6,*], Maosheng He[2], Jianfei Wu[3,4], Hailun Ye[3,4], Tingdi Chen[3,4], Jian Li[3,4], Jie Zeng[3,4], Zonghua Ding[7], Na Li[8], Jian Wang[9], Robert A. Vincent[10], Iain M. Reid[10,11], Paulo P. Batista[12], Ricardo A. Buriti[13], Toshitaka Tsuda[14], Nicholas J. Mitchell[15,16], Xiankang Dou[5]

[1]School of Microelectronics, Tianjin University, Tianjin, China
[2]Sate Key Laboratory of Solar Activity and Space Weather, National Space Science Center, Chinese Academy of Sciences, Beijing, China
[3]School of Earth and Space Sciences, University of Science and Technology of China, Hefei, China
[4]CAS Center for Excellence in Comparative Planetology, Anhui Mengcheng Geophysics National Observation and Research Station, University of Science and Technology of China, Hefei, China
[5]Hefei National Laboratory, University of Science and Technology of China, Hefei, China
[6]Collaborate Innovation Center of Astronautical Science and Technology, Harbin, China
[7]Kunming Electro-Magnetic Environment Observation and Research Station, Qujing, China
[8]School of Electronic Science and Technology, Hainan University, Haikou, China
[9]School of Electrical and Electronic Engineering, North China Electric Power University, Beijing
[10]School of Physical Sciences, University of Adelaide, Adelaide, South Australia, Australia
[11]ATRAD Pty Ltd., Underdale, South Australia, Australia
[12]National Institute for Space Research, S. J. dos Campos, Brazil
[13]Federal University of Campina Grande, PB, Brazil
[14]Research Institute for Sustainable Humanosphere (RISH), Kyoto University, Uji, Kyoto, Japan
[15]Department of Electronic and Electrical Engineering, University of Bath, Bath, UK
[16]British Antarctic Survey, Cambridge, UK
Correspondence to: Xianghui Xue (xuexh@ustc.edu.cn) and Wen Yi (yiwen@ustc.edu.cn)

Abstract. Horizontal winds from six meteor radars during 2005–2012 are used to derive nonmigrating tides in the mesosphere and lower thermosphere (MLT). To our knowledge, it is the first time to derive dominant nonmigrating tides from sparse meteor radar observations. The radars are located at Cariri (7.4° S, 36.5° W), Kototabang (0.2° S, 100.3° E), Ascension Island (7.9° S, 14.4° W), Darwin (12.3° S, 130.8° E), Buckland Park (34.6° S, 138.5° E), and Kunming (25.6°N, 103.8°E). Tidal fitting simulations based on the Whole Atmosphere Community Climate Model (WACCM) winds indicate that DW1, DE3, DE2, and DW2 can be accurately decomposed from these radars. The dominant nonmigrating tides, DE3, DE2, and DW2, show pronounced seasonal and altitudinal variations, and their dominant Hough mode components are identified. The climatology of these tides is consistent with the Climatological Tidal Model of the Thermosphere (CTMT) output. During the 2006 stratospheric sudden warming (SSW) event, DE3 was suppressed during SSW development and recovered after SSW dissipation; DE2 was enhanced during SSW development and rapidly suppressed after SSW reach the maximum; DW2 was

https://doi.org/10.5194/egusphere-2026-6900
Preprint. Discussion started: 12 November 2026
© Author(s) 2026. CC BY 4.0 License.



suppressed near the SSW central day and strongly enhanced 20 days later. This study develops a method to decompose dominant nonmigrating tidal winds by jointly analyzing six meteor radars and provides an observational basis for modeling tidal dynamics in the MLT and for investigating middle atmosphere-ionosphere coupling through nonmigrating tides.

Short Summary. Horizontal winds from six meteor radars in the low-latitude region are used to derive nonmigrating tides in the MLT. To our knowledge, it is the first time to decompose nonmigrating tides from sparse meteor radar observations. The climatology of DE3, DE2, and DW2 is consistent with CTMT. During the 2006 SSW, these tides show significant response. This study develops a method for decomposing nonmigrating tidal winds and provides a chance for investigating middle atmosphere–ionosphere coupling.

1 Introduction

Dynamic process in the mesosphere and lower thermosphere (MLT) region plays a critical role in the coupling between the lower atmosphere and the thermosphere/ionosphere system. The dynamics in the MLT region are primarily modulated by atmospheric waves (such as gravity waves, tides, and planetary waves) generated in the lower atmosphere; as these waves propagate upward, the influence of lower atmospheric activity can be imprinted onto the variability in the middle and upper atmosphere. The atmospheric waves also can alter the distribution of ionospheric plasma through collisions between neutral atmospheric molecules and plasma, as well as through the dynamo effect. Therefore, an understanding of these processes is necessary for studies of the thermosphere and/or ionosphere with regard to space weather. Among them, atmospheric tides are significant waves that can dominate the dynamics in the MLT region.

Atmospheric tides are global-scale atmospheric oscillations with periods that are harmonics of a solar day (Chapman and Lindzen, 1970). According to the feature of their zonal propagation, the atmospheric tides can be classified as either migrating or nonmigrating tides. Migrating tides propagate westward with the apparent motion of the sun, whereas nonmigrating tides can propagate westward/eastward or remain stationary. Nonmigrating tides are primarily excited by latent heat release associated with deep convection and nonlinear interactions between planetary waves and migrating tides (Oberheide et al., 2002; Miyoshi et al., 2017). Nonmigrating tides can alter the momentum and energy of the zonal mean flow, greatly changing middle atmosphere dynamics (Isoda et al., 2004). Nonmigrating tides also play an important role in middle atmosphere–ionosphere coupling. Through the E-region dynamo effect, they can modify the distribution of ionospheric plasma, such as the wave-4 structure induced by diurnal tides with eastward propagating zonal wavenumber 3 (DE3; He et al., 2011; Nischal et al., 2019; Zhou et al., 2024; Liao et al., 2026).

Traditionally, observations of global atmospheric tides have been investigated using satellites (Forbes et al., 2008; Wu et al., 2006, 2008, 2011; Xu et al., 2009, 2012; Yue et al., 2013). However, due to the limitations of satellite orbits, it is difficult to independently extract day-to-day variability of migrating and nonmigrating tides. Li et al. (2015) developed a method to extract day-to-day nonmigrating tides from TIMED/SABER satellite temperature and investigated the variability of the diurnal nonmigrating tidal component DE3 and the semidiurnal nonmigrating tidal component SE2 (Li et al., 2017, 2019a, 2020, 2022). Based on this method, Li et al. (2019b) presented correlations between the ionospheric

https://doi.org/10.5194/egusphere-2026-6900
Preprint. Discussion started: 12 November 2026
© Author(s) 2026. CC BY 4.0 License.

wave-4 structure and the DE3 tide in the upper atmosphere on meteorological timescales shorter than 60 days.

However, current mainstream middle and upper atmosphere satellites provide temperature observations rather than wind measurements. Tidal winds are important in middle atmosphere–ionosphere coupling, as they can drive the E-region dynamo effect. Meteor radars can provide local site, high temporal resolution, and continuous horizontal wind observations in the MLT (Stober et al., 2020, 2021; Dempsey et al., 2021; Griffith et al., 2021; Liu et al., 2022). However, these studies are all based on single stations and cannot resolve the global-scale structure of tides. To obtain nonmigrating tidal winds, a few studies have combined a suitable longitudinal distribution of ground-based radars. Murphy et al. (2003, 2006) derived semidiurnal tides with westward propagating zonal wavenumber 1 and 2 (SW1 and SW2) via six medium frequency (MF) radars in Antarctica. He et al. (2018, 2019) reported a method to decompose the semidiurnal tides with different zonal wavenumber and lunar tides from several meteor radars located at mid-latitudes with similar latitudes but different longitudes. These studies are primarily focused on high latitudes because of the rich coverage of ground-based radars. Nevertheless, due to the complexity of tidal components at low latitudes and the sparse distribution of stations, this method cannot be directly applied to decompose migrating and nonmigrating tidal components at low latitudes. In addition, investigating nonmigrating tides in the low-latitude MLT region is important and necessary because they make major contributions to the E-region dynamo effect.

Based on the questions raised by the studies noted above, in this study, we develop a method to decompose nonmigrating tides via the horizontal mesospheric winds observed by six meteor radars in the low-latitude region. We analyze the feasibility of tidal fits by using horizontal winds from the Whole Atmosphere Community Climate Model (WACCM), and compare the climatology of these tidal components between meteor radar observations and the Climatological Tidal Model of the Thermosphere (CTMT). As a case analysis, the response of these nonmigrating tidal components to the 2006 stratospheric sudden warming (SSW) is also investigated. Section 2 provides the data employed and the methodology developed in this study; section 3 presents the observational results of three dominant nonmigrating tidal components; and the discussion and conclusions are provided in sections 4 and 5, respectively.

2 Data and Methodology

2.1 Meteor radars

Six meteor radars located at Cariri, Brazil (7.4° S, 36.5° W), Kototabang, Indonesia (0.2° S, 100.3° E), Ascension Island, United Kingdom (7.9° S, 14.4° W), Darwin, Australia (12.3° S, 130.8° E), Buckland Park, Australia (34.6° S, 138.5° E), and Kunming, China (25.6°N, 103.8°E) denoted respectively CMR, KMR, AMR, DMR, BPMR, and KMMR, are used to measure the neutral horizontal winds. The horizontal winds observed from these six meteor radars are utilized for the decomposition of mesospheric nonmigrating tides. The operating frequencies, geographic coordinates, observational time periods, altitude ranges, as well as temporal and altitudinal resolutions of the six meteor radars are summarized in Table 1.

Table 1: Geographic locations, system parameters and observational time periods of the meteor radars used in this study.

https://doi.org/10.5194/egusphere-2026-6900
Preprint. Discussion started: 12 November 2026
© Author(s) 2026. CC BY 4.0 License.

Meteor radar	Geographic locations	Operation frequency	Altitude range	Altitudinal resolution (km)	Temporal resolution (hour)	Data used in this study
Cariri (CMR)	7.4° S, 36.5° W	35.2 MHz	81–99 km	3.0	1	1/1/2005–12/31/2008
Kototabang (KMR)	0.2° S, 100.3° E	37.7 MHz	80–100 km	2.0	1	1/1/2005–12/31/2012
Darwin (DMR)	12.3° S, 130.8° E	33.2 MHz	80–100 km	2.0	1	1/1/2005–12/31/2012
Ascension Island (AMR)	7.9° S, 14.4° W	43.5 MHz	80–100 km	2.0	1	1/1/2005–12/31/2012
Buckland Park (BPMR)	34.6° S, 138.5° E	31 MHz	80–100 km	2.0	1	1/1/2006–12/31/2012
Kunming (KMMR)	25.6° N, 103.8° E	37.5 MHz	80–100 km	2.0	1	7/29/2008–12/31/2012

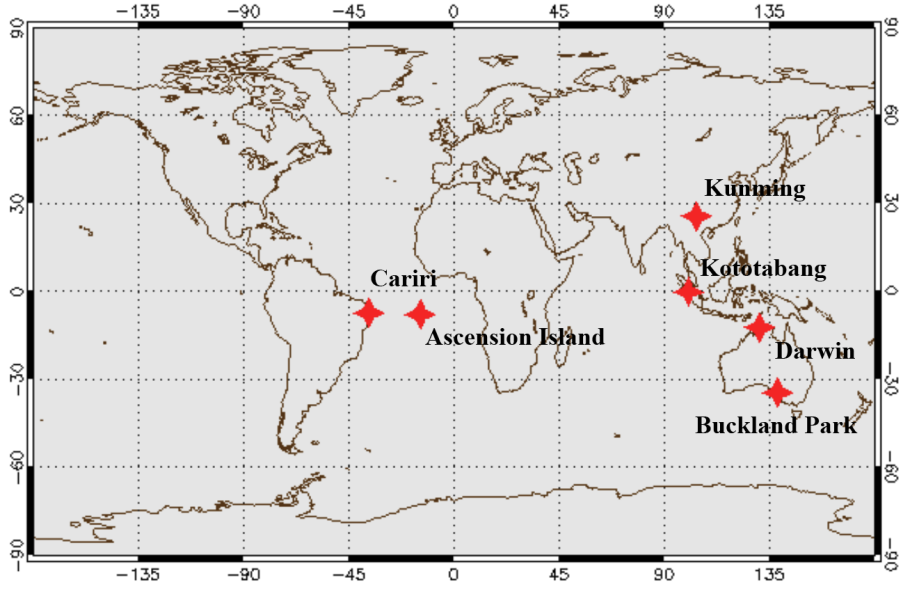


Figure 1: The geographic locations of the six meteor radars used in this study.

The radar system operates by transmitting the radio wave and coherently detecting the meteor trail reflections. The cross-dipole Yagi antennas are employed for both transmission and reception. The range

https://doi.org/10.5194/egusphere-2026-6900
Preprint. Discussion started: 12 November 2026
© Author(s) 2026. CC BY 4.0 License.

is derived from the time delay between signal transmission and detection, while the azimuth and zenith angles are obtained from the phase differences between receiving antennas. Under the Assumption that the vertical wind is negligible, the horizontal wind can be determined by the Doppler shift using the algorithms described by Hocking et al. (2001) and Holdsworth et al. (2004).

2.2 SD-WACCM-X

SD-WACCM-X is an advanced numerical model developed within the Community Earth System Model version 1 (CESM1) framework (Hurrell et al., 2006). It is specifically designed to investigate the coupling among chemistry, radiation, and dynamics and their impact on the Earth's climate system (Neale et al., 2013). The SD-WACCM-X version 2.1 simulation from the surface up to approximately 50 km is nudged from Modern-Era Retrospective analysis for Research and Applications, Version 2 (MERRA-2) data. In this study, the 3-hourly SD-WACCM-X modelling is employed to obtain the nonmigrating tidal components in the neutral horizontal winds in the MLT region and ionosphere.

2.3 CTMT

The Climatological Tidal Model of the Thermosphere (CTMT) is constructed using TIDI, SABER and Challenging Minisatellite Payload (CHAMP) dataset, as proposed and developed by Oberheide et al. (2011). This model is operating in three dimensions of latitude (from 90° S to 90° N), altitude (from 80 km to 400 km), and month (from January to December), which is based on tidal observations made in the MLT region that are extended into the thermosphere using Hough mode extension (HME) modeling. The observation data comprise the TIDI zonal and meridional wind tides, SABER temperature tides and CHAMP neutral density tides in the 2002 to 2008 composite years. The CTMT provides the 14 most significant diurnal and semidiurnal tidal components for temperature, density, and zonal, meridional and vertical winds, including DW2, DW1, D0, DE1, DE2, DE3, SW4, SW3, SW2, SW1, S0, SE1, SE2, and SE3. In addition, CTMT is valid only for 110 solar flux units (sfu) due to the tidal dissipation sensitivity to thermospheric temperature.

2.4 Approach for tidal decomposition

In principle, the time series of hourly zonal and meridional winds observed by meteor radars within six geographic longitudinal sectors can be employed to derive the amplitude and phase characteristics of diurnal, semidiurnal, and terdiurnal tides, with different zonal wavenumbers. Given that the DE3 and/or DE2 tidal components are strong candidates for the dominant nonmigrating tidal components affecting ionospheric wave-like structures (e.g., He et al., 2011, Liao et al., 2026), it is necessary to extend the decomposition functions to at least eastward-propagating wavenumber 3. A least square fitting performed on the hourly wind data for each 3-day sliding window throughout the series could be used to decompose the migrating and nonmigrating tidal components, following the above function (Baumgarten and Stober, 2019; Wang et al., 2022, 2025).

$$u(\mathrm{z},\lambda,\mathrm{t}) = u_0(z) + \sum_{n=1}^{3}\sum_{s=-3}^{3}[a_{n,s}(z)\sin\left(\frac{2\pi n}{T}t + s\lambda\right) + b_{n,s}(z)\cos\left(\frac{2\pi n}{T}t + s\lambda\right)], \quad (1)$$

where u denotes either the zonal or meridional wind; z denotes altitude; t denotes universal time; λ denotes longitude (rad); n denotes temporal wavenumber; s denotes zonal wavenumber; T indicates 24

https://doi.org/10.5194/egusphere-2026-6900
Preprint. Discussion started: 12 November 2026
© Author(s) 2026. CC BY 4.0 License.

hours; and u_0 denotes zonal mean zonal wind or zonal mean meridional wind.

It is noted that the largest difference of latitude with each radar is up to ~60°. Thus, Therefore, it is necessary to introduce Hough functions for the fitting procedure.

$$\boldsymbol{u(z,\phi,\lambda,t) = u_0(z) + \sum_{n=1}^{2}\sum_{s=-3}^{3}\sum_{m=|s|}^{|s|+4}[a_{n,s,m}(z)\,sin(n\Omega t + s\lambda)_{s,m}^{n}\Theta(\phi) + b_{n,s,m}(z)cos(n\Omega t + s\lambda)_{s,m}^{n}\Theta(\phi)]}, \quad (2)$$

where ϕ denotes latitude (rad); ${}_{s,m}^{n}\Theta(\phi)$ indicates the (s, *m*) Hough mode with frequency of *n*. To mitigate spatial aliasing effects caused by spectral leakage from higher parameters into lower ones, our methodology incorporates additional Hough modes of *m* from |s| to (|s|+4) into the decomposition functions. These Hough modes are calculated by Chebyshev collocation method (Orszag, 1974; Boyd, 1978; Wang et al., 2016).

The matrix forms of Equation (2) can be written as

$$\begin{bmatrix} sin\left(\frac{2\pi}{T}t_1 - 3\lambda_1\right)_{-3,3}^{1}\Theta(\phi_1) & \cdots & sin\left(2\times\frac{2\pi}{T}t_1 + 3\lambda_1\right)_{3,7}^{2}\Theta(\phi_1) \\ \vdots & \ddots & \vdots \\ sin\left(\frac{2\pi}{T}t_{72} - 3\lambda_6\right)_{-3,3}^{1}\Theta(\phi_6) & \cdots & sin\left(2\times\frac{2\pi}{T}t_{72} + 3\lambda_6\right)_{3,7}^{2}\Theta(\phi_6) \end{bmatrix}$$

$$\begin{bmatrix} cos\left(\frac{2\pi}{T}t_1 - 3\lambda_6\right)_{-3,3}^{1}\Theta(\phi_1) & \cdots & cos\left(2\times\frac{2\pi}{T}t_1 + 3\lambda_1\right)_{3,7}^{2}\Theta(\phi_1) & 1 \\ \vdots & \ddots & \vdots & \vdots \\ cos\left(\frac{2\pi}{T}t_{72} - 3\lambda_6\right)_{-3,3}^{1}\Theta(\phi_6) & \cdots & cos\left(2\times\frac{2\pi}{T}t_{72} + 3\lambda_6\right)_{3,7}^{2}\Theta(\phi_6) & 1 \end{bmatrix}\begin{bmatrix} a_{1,-3,3} \\ \vdots \\ a_{2,3,7} \\ b_{1,-3,3} \\ \vdots \\ b_{2,3,7} \\ u_0 \end{bmatrix} =$$

$$\begin{bmatrix} u(z_0,\phi_1,\lambda_1,t_1) \\ \vdots \\ u(z_0,\phi_6,\lambda_6,t_{72}) \end{bmatrix}, \quad (3)$$

The first matrix on the left side of the equal sign in Equation (3) is denoted as $\boldsymbol{A}$, which is the coefficient matrix for tidal decomposition with dimensions of 432×141. The second matrix is referred to as $\boldsymbol{x}$, representing the vector of the tidal components; it has dimensions of 141×1, with each element being a distinct variable to be solved. The matrix on the right side of the equal sign is denoted as $\boldsymbol{b}$, containing horizontal wind observations at different longitudes, latitudes and times, and its dimensions are 432×1. Equation (3) can then be expressed as

$$\boldsymbol{Ax = b}, \quad (4)$$

This system comprises 141 unknown coefficients. For each 3-day temporal and 2-km altitudinal window, there are 432 equations based on the amount of available data, allowing for a solution attempt. However, due to the sparse distribution of observation stations, these equations are not mutually independent; there are basically 15 unknown coefficients related to the longitude, but only 6 meteor radars at different longitudes are contributing to the solution. Consequently, solving this system is essentially an underdetermined linear problem, yielding non-unique solutions. To obtain a unique solution set, additional constraints must be introduced.

Considering the physical feature of atmospheric tides, their spectral and wavenumber distributions are discrete, with only a limited number of components exhibiting significant amplitudes. Therefore, even if it is not possible to extract all potential tidal components, it is feasible to extract the most prominent ones. In other words, the vector $\boldsymbol{x}$, which contains information on the tidal components, can be defined as the

https://doi.org/10.5194/egusphere-2026-6900
Preprint. Discussion started: 12 November 2026
© Author(s) 2026. CC BY 4.0 License.

solution to the following optimization problem

$$\begin{aligned} &minimize && ||\boldsymbol{x}||_0 \\ &subject\ to: && \boldsymbol{Ax} = \boldsymbol{b}' \end{aligned} \tag{5}$$

where $||\boldsymbol{x}||_0$ is defined as the number of non-zero entries in the vector $\boldsymbol{x}$, which is referred to the zero norm of vector $\boldsymbol{x}$.

To solve the optimization problem in Equation (5), this work adopts a sparse reconstruction algorithm, the Optimized Orthogonal Matching Pursuit (OOMP) algorithm (Rebollo-Neira and Lowe, 2002) to decompose the migrating and nonmigrating tidal components. As an enhancement over the classical Orthogonal Matching Pursuit (OMP) algorithm, widely employed in compressed sensing for sub-Nyquist signal recovery, the OOMP improves accuracy and stability by virtue of its orthogonal projection, which guarantees optimal selection at each step and reduces the need for matrix inversion. The procedure iteratively selects the candidate component most correlated with the current residual, thereby incrementally reconstructing the sparse signal. The iteration continues until the residual diminishes below the wind measurement error or until all candidate components have been selected.

2.5 Credibility of the method used to calculate tidal components

The sparse reconstruction algorithm is applied for the first time to the separation of atmospheric wave modes. To evaluate the credibility of this algorithm, simulation tests are considered. The first test examines whether the algorithm can effectively identify the dominant tidal components. Zonal wind velocities are set as the superposition of different tidal modes, with a random error of 5 m/s taken into account. Diurnal and Semidiurnal components from eastward-propagating 3 (E3) to westward-propagating 3 (W3) are considered, which the dominant components, amplitudes, and phases of the tides are all randomly generated. A dominant component is defined as a tidal component which amplitude is larger than twice the maximum random error (10 m/s). The number of dominant components is defined as the maximum between the number of dominant diurnal tidal components and the number of dominant semidiurnal tidal components, because the meteor observational data are sparse only in the longitudinal dimension. For example, a dominant component count of seven indicates that the amplitudes of all tidal components from E3 to W3 are larger than 10 m/s. Figure 2a presents the probability that the algorithm accurately computes all dominant components under different counts of dominant components (10,000 simulations are performed for each count). "Accurate computation" requires meeting the following conditions: (1) inclusion of all dominant components; (2) consistency in the order of the retrieved amplitudes with that of the prescribed wind speeds; (3) errors in the retrieved amplitudes and phases not exceeding 5 m/s. As shown in Figure 2a, when the count of dominant components is one or two, the probability of accurately computing the dominant tidal components approaches 100% and 99.15%; when the count is less than seven, the probability exceeds 68.19%.

https://doi.org/10.5194/egusphere-2026-6900
Preprint. Discussion started: 12 November 2026
© Author(s) 2026. CC BY 4.0 License.

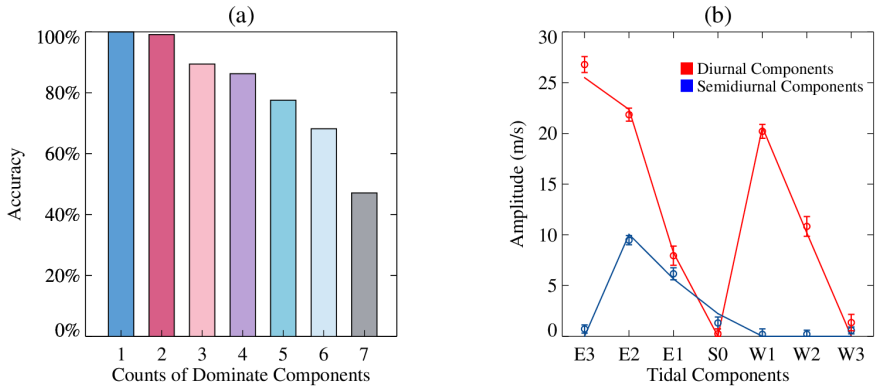


Figure 2: (a) Probability that the algorithm can accurately compute the dominant tidal components, based on results from 10,000 simulations for each count. (b) The comparison between the set parameters of one of the simulation tests and their calculated results. These results were obtained from 1000 repeated calculations using the present method under a wind-velocity error of 5 m/s. The red (blue) solid lines denote the set values of diurnal (semidiurnal) tidal amplitudes. The red (blue) circles and error bars denote the decomposed amplitudes and standard deviations of diurnal (semidiurnal) tides, respectively.

As an example, Figure 2b presents the results of one of the simulation tests. Similar to the real-world physical situation in the low-latitude MLT region, the relative magnitudes of the different diurnal tidal components are such that DE3, DE2, and DW1 are the strongest, followed by DW2 and DE1, while DS0 and DW3 are very weak. The amplitudes of DE3, DE2, DW1, DW2, DE1, DS0, and DW3 are set as 25.5 m/s, 22.4 m/s, 8.2 m/s, 0 m/s, 20.6 m/s, 10.2 m/s, and 0 m/s, respectively. The semidiurnal tidal components are set to SE2, SE1, and SS0 with amplitudes of 10.0 m/s, 5.6 m/s, and 2.2 m/s, respectively, and other components, which are not consistent with the actual conditions. The calculated amplitudes of the diurnal (semidiurnal) tides are denoted by red (blue) circles, respectively, in Figure 2b. For the diurnal components from DE3 to DW3, the results are 26.79 m/s, 21.85 m/s, 7.95 m/s, 0.25 m/s, 20.21 m/s, 10.83 m/s, and 1.35 m/s, respectively. For the semidiurnal components from SE3 to SW3, the amplitudes are 0.72 m/s, 9.47 m/s, 6.17 m/s, 1.31 m/s, 0.19 m/s, 0.20 m/s, and 0.58 m/s, respectively. The uncertainties are indicated by error bars, with all values being less than 1 m/s.

This result indicates that the calculated values closely preserve the order of magnitude of the input values, meaning that the five main components of the diurnal tide (DE3, DE2, DW1, DW2, and DE1) and the three main components of the semidiurnal tide (SE2, SE1, and SS0) were effectively decomposed. For the tidal components with zero set amplitudes, the maximum calculated value is 1.35 m/s (for DW3), with all others below 1 m/s. Furthermore, for the major tidal components, the largest difference between the set and calculated amplitudes is 1.29 m/s (for DE3), which is far smaller than the maximum simulation error of 5 m/s. This example indicates that, using wind time series at the given six geographic longitudes and latitudes, the proposed method can effectively decompose the dominant diurnal and semidiurnal components. In the situation that the maximum wind-speed error was not exceeded 5 m/s, the calculating error can be confined well below 1.35 m/s (in this test). Therefore, our proposed method can be applied to wind observations from these six radar stations to reliably obtain the major tidal components.

https://doi.org/10.5194/egusphere-2026-6900
Preprint. Discussion started: 12 November 2026
© Author(s) 2026. CC BY 4.0 License.

To further analyze the credibility of the proposed method, a high-resolution model will be considered. WACCM is considered in this study, as a model with high temporal and spatial resolution and satisfactory credibility for neutral winds in the MLT region, and it could be used to simulate the decomposed calculation of MLT tides (Pedatella et al., 2012a; Smith et al., 2017; Yang et al., 2018; Stober et al., 2021). WACCM is a high-top model based on the Community Earth System Model (version 1) framework (Hurrell et al., 2006), which is an optional variation of the Community Atmosphere Model version 4 (CAM4) that has been designed to investigate the interactions among chemistry, radiation, and dynamics and their impact on the Earth's climate system (Neale et al., 2013). The current study uses the specific dynamics (SD) version of WACCM, in which neutral temperatures and winds below 50 km are nudged toward NASA's Modern-Era Retrospective analysis for Research and Applications (MERRA) (Lamarque et al., 2012). The present integrations have a horizontal resolution of 2.5° in longitude and 1.9° in latitude. There are 144 vertical levels, and the vertical resolution is approximately 0.5 km, ranging from 80 to 100 km. The time step is 30 minutes.

Figures 3a–3f present the decomposed result of DW1, DE3 and DE2 amplitudes in both zonal and meridional components at the latitude of 5° S based on the hourly zonal and meridional wind over six selected longitudinal-latitudinal sectors from the WACCM output. As a comparison, Figures 3g–3l show the DW1, DE3 and DE2 amplitudes derived from a least-square fitting, by using the WACCM hourly wind data from all longitudes at 5° S. The least-square fitting used in Figures 3g–3l is performed on the WACCM wind data for each 3-day sliding window. Considered that the WACCM zonal and meridional wind data are available on a global scale and have 144 different longitudes, the zonal wavenumber is taken from eastward-propagating 7 to westward-propagating 7 for calculating all diurnal tidal components. Following the above least-square fitting method, the meridional or zonal wind variations in time and longitude at a given altitude can be written as follows:

$$u(z,\lambda,t) = u_0(z) + \sum_{n=1}^{2}\sum_{s=-7}^{7} c_{n,s}(z)\cos\left(\frac{2\pi n}{T}t + \frac{2\pi s}{2\pi}\lambda + \varphi_{n,s}(z)\right), \quad (6)$$

where u represents either the zonal or meridional wind; z represents altitude; t represents time; λ represents longitude (rad); n represents temporal wavenumber; s represents zonal wavenumber; T equals 24 hours; φ represents phase; u_0 represents background zonal (or meridional) wind; the second section represents tidal components comprising 24- and 12-hour oscillations.

https://doi.org/10.5194/egusphere-2026-6900
Preprint. Discussion started: 12 November 2026
© Author(s) 2026. CC BY 4.0 License.

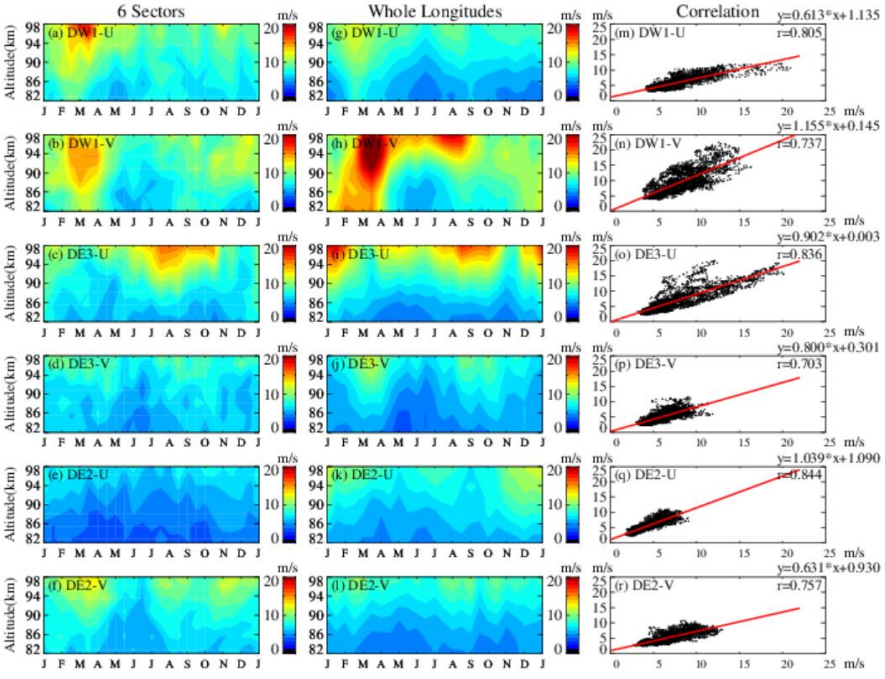


Figure 3: (a–f) The climatology of DW1, DE3, and DE2 amplitudes in both zonal and meridional components at 5° S in the altitudinal range of 82-98 km, decomposed by the hourly zonal and meridional wind over six selected longitudinal-latitudinal sectors (the same as the geographic locations of the six radars used in this study) from the WACCM output. (g–l) The climatology of DW1, DE3, and DE2 amplitudes in both zonal and meridional components in the altitudinal range of 82-98 km, derived from a least-square fitting, based on the WACCM hourly wind data from all longitudes at 5° S. (m–r) The correlation between the six-sector fitting (the OOMP method based on six-sector data) and whole-longitude fitting (the least-square fitting based on whole-longitude data) for DW1, DE3 and DE2 tidal amplitudes in both wind component obtained from WACCM. The horizontal axis gives the values calculated from the six-sector fitting, while the vertical axis gives those from the whole-longitude fitting. Each black dot corresponds to a daily value at a given altitude. The red solid line is the least-squares linear regression line calculated by all black dots, indicating the overall correlation and slope. (D: Diurnal tides; E: Eastward propagation; W: Westward propagation)

As shown in Figure 3, for the diurnal components of DW1, DE3 and DE2, the seasonal variations derived from the proposed method by six-sector data exhibit strong consistency with those from the whole-longitude fitting, with only minor differences in amplitude. Specifically, the results of six-sector fitting show slightly larger amplitudes for DW1-U, while those for DW1-V and DE2-U are opposite. In terms of amplitude, the results calculated via both methods consistently show that DE3 and DW1 have the largest amplitudes, followed by DE2. In addition, correlation analysis indicates that the results obtained from the two methods are highly correlated for DW1, DE3, and DE2, with the Pearson correlation coefficients over 0.7. Among these, the correlations for the zonal components (all above 0.8) are

https://doi.org/10.5194/egusphere-2026-6900
Preprint. Discussion started: 12 November 2026
© Author(s) 2026. CC BY 4.0 License.

consistently higher than those for the meridional components (all below 0.8). For both wind components, DE2 exhibits the highest correlation, while DW1 and DE3 show slightly lower values.

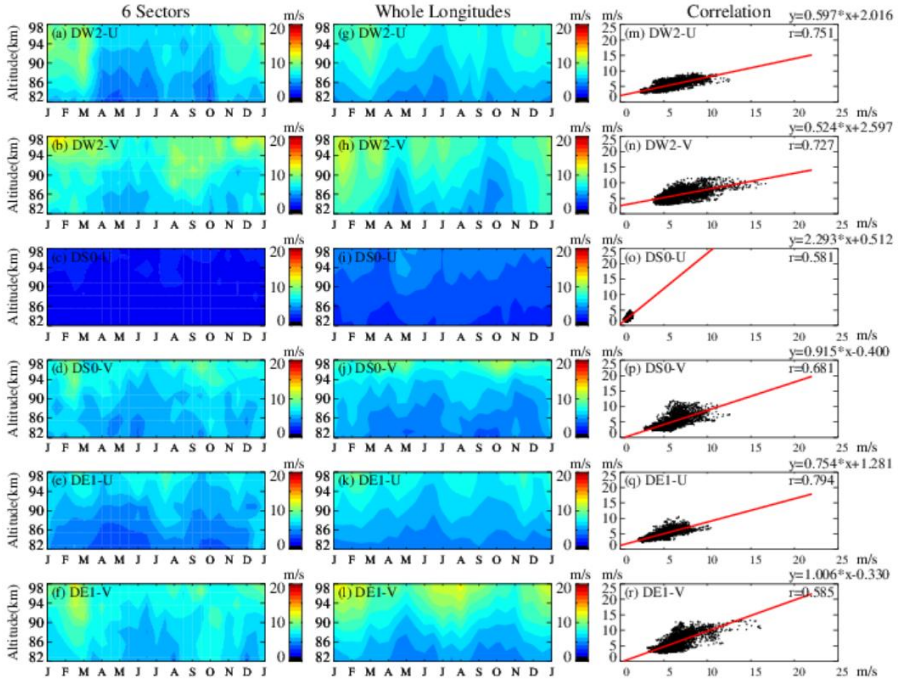


Figure 4: The same as Figure 3, but for DW2, DS0 and DE1.

Figure 4 also shows the comparing results for DW2, DS0 and DE1. For these three components, only DW2 shows consistent seasonal variations between the two methods in both zonal and meridional components. For DS0-U, it is virtually impossible to be identified as a valid component in six-sector fitting. For DE1-V, the seasonal variations obtained from the two methods differ considerably. In terms of amplitude, DS0 and DE1 are the smallest among all the components considered, compared with DE3, DE2, DW1, and DW2. DW3 is not shown here because it was not output in the CTMT used for subsequent analysis and also exhibits poor accuracy. Regarding correlation, the correlation coefficients for DE3, DE2, DW1, and DW2 are above 0.7 in both zonal and meridional components, while the correlation coefficients for DS0 and DE1 show relatively lower correlations. Therefore, the primary components that can be reliably decomposed by the present method (equation 5) are DE3, DE2, DW1, and DW2. In the subsequent analysis, only the nonmigrating tides DE3, DE2, and DW2 are considered, while the other nonmigrating tidal components are excluded.

In addition, since an additional zero norm minimization constraint has been incorporated into the present method, energy from some minor components will tend to leak into some major components. This situation may lead to overestimation of some major components and underestimation of some minor components. As shown in Figures 3 and 4, the amplitudes of DW1-U, DE3-U, DE3-V, DE2-V, DW2-U, DW2-V, DS0-V, and DE1-U have been slightly overestimated, as well as the amplitudes of DW1-V, DE2-U, DS0-U, and DE1-V have been slightly underestimated. Among them, for the major components of DE3, DE2, DW1, and DW2, the total amplitudes of DE3-U and DE2-U exist less difference, with the

https://doi.org/10.5194/egusphere-2026-6900
Preprint. Discussion started: 12 November 2026
© Author(s) 2026. CC BY 4.0 License.

ratio of 0.902 and 1.039 (whole-longitude fitting vs. six-sector fitting), respectively. The overestimation of DW2-V is largest, almost twice those of whole-longitude fitting values (with the ratio of 0.524). The overestimations of DW1-U, DW2-U, DE3-V, and DE2-V are less pronounced, with the largest factor not exceeding 1.6 (corresponding to the ratio of 0.625). Only DW1-V amplitude is underestimated, by a factor of approximately 0.86 (corresponding to the ratio of 1.155).

3 Results

To derive the nonmigrating tides, the meteor winds were jointly analyzed by equation (5) to calculate amplitudes for all dominant tidal components.

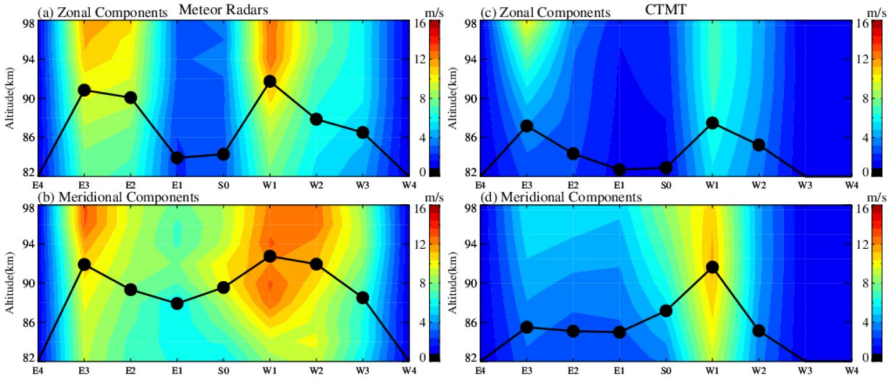


Figure 5: (a–b) Zonal wavenumber-altitude spectrum of diurnal tides from eastward-propagating 4 (E4) to westward-propagating 4 (W4) at the latitude of 5°S in the altitude range of 82–98 km, averaged over the entire observation period, based on meteor radar observations in the (a) zonal and (b) meridional components. (c–d) Same as (a–b), but from CTMT outputs. The solid black dots denote the altitude-averaged amplitude for each zonal wavenumber.

Figure 5 presents the comparison of the zonal wavenumber-altitude spectrum for diurnal tides between meteor radar observations and CTMT outputs. It is shown that, in both the radar observations and the CTMT simulations over the 5°S region, the DE3 and DW1 components are the most prominent. For all tidal components, the amplitudes increase with altitude, which is consistent with our knowledge. In the calculation from the meteor radar zonal winds, DW1, DE3, and DE2 are the strongest, followed by DW2 and DW3, while DS0 and DE1 remain weakest. This order is consistent with the CTMT outputs, although the observational amplitudes are slightly larger than the model results. For the meridional component, DE1 and DS0 are also the weakest, but they are slightly stronger than those in zonal components, which is also consistent with the CTMT outputs. Based on the credibility analysis of the proposed method presented in the previous subsection, only dominant components can be reliably derived. Therefore, the subsequent analysis is primarily focused on the dominant nonmigrating tidal components, DE3, DE2, and DW2. Also, the meteor observational results for the other nonmigrating components (DE1, DS0, and DW3), as well as the migrating tides (DW1), are provided in Figure A1.

https://doi.org/10.5194/egusphere-2026-6900
Preprint. Discussion started: 12 November 2026
© Author(s) 2026. CC BY 4.0 License.

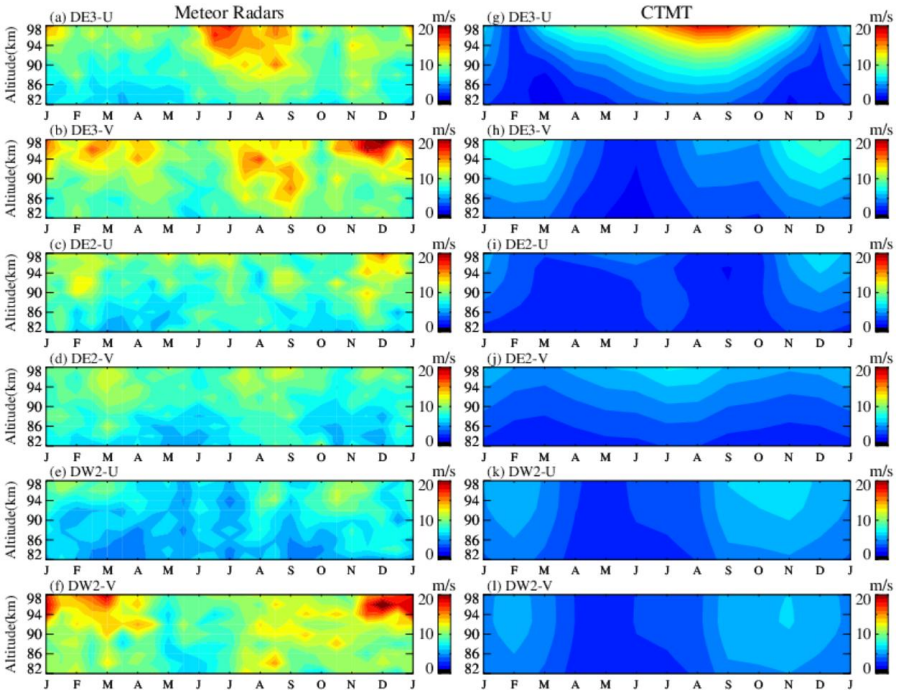


Figure 6: (a–f) The seasonal variation of DE3, DE2, and DW2 amplitudes in both zonal and meridional components at 5° S in the altitudinal range of 82–98 km, decomposed by the hourly zonal and meridional wind over six meteor radars. (g–l) Same as (a–f), but from CTMT outputs.

The climatology of DE3, DE2, and DW2 amplitudes in both zonal and meridional components in the 5° S MLT region is shown in Figure 6. In the observational results, the amplitude of DE3 in zonal component (DE3-U) reaches its maximum during June–August each year, with a secondary maximum in January. For DE3 in meridional component (DE3-V), the amplitude exhibits three pronounced maximum each year, occurring in January–April, July–September, and November–January, with the weakest amplitudes observed during May–June. The amplitude of DE2-U is strong during the summer (June–July) and the winter (November–February), with the wintertime maximum being the strongest, and is weak during the equinox periods (April and October). The seasonal variation of DE2-V is generally similar to that of DE2-U, but with the strongest amplitude occurring in summer. For DW2-U, the amplitude reaches its peak during January–February, August, and September–December, while the minimum occurs during April–June. The seasonal variation of DW2-V is consistent with that of DW2-U, and the amplitude of DW2-V is slightly larger.

In the CTMT outputs, the seasonal variations of the DE3, DE2, and DW2 tides in both zonal and meridional components are well consistent with the observational results. The primary difference between the two results is that the observed amplitudes are all slightly larger than the CTMT outputs; except for DE3-U, the observed amplitudes of the other components are roughly twice those of the CTMT outputs. According to the simulation in section 2.5 (as shown in Figures 3 and 4), all major nonmigrating components except DE3-U and DE2-U are overestimated to varying extents (by factors of ~1.2–1.9), due to limitations inherent in the calculation method. This can only partially account for the approximately

https://doi.org/10.5194/egusphere-2026-6900
Preprint. Discussion started: 12 November 2026
© Author(s) 2026. CC BY 4.0 License.

twice the amplitude difference; moreover, the CTMT outputs may also underestimate the MLT tidal winds. In previous studies, meteor radar observations of migrating tides have also been found to be slightly larger than CTMT outputs (Wang et al., 2022). Unlike migrating tides, the nonmigrating tidal winds in CTMT are directly derived from TIDI wind data (Oberheide et al., 2011). Some previous studies have suggested that tidal winds measured by the TIDI instrument are smaller than those from meteor radar measurements in the low-latitude region (Ward et al., 2010; Kumar et al., 2014; Paulino et al., 2025), with a larger discrepancy in the meridional winds (Gauthier et al., 2025), which may account for the larger nonmigrating tidal amplitudes observed by meteor radars.

4 Discussion

4.1 The latitudinal features of nonmigrating tides

Since Hough modes are used as the orthogonal basis in the present method, it enables the latitudinal variation features of different tidal components to be obtained and discussed.

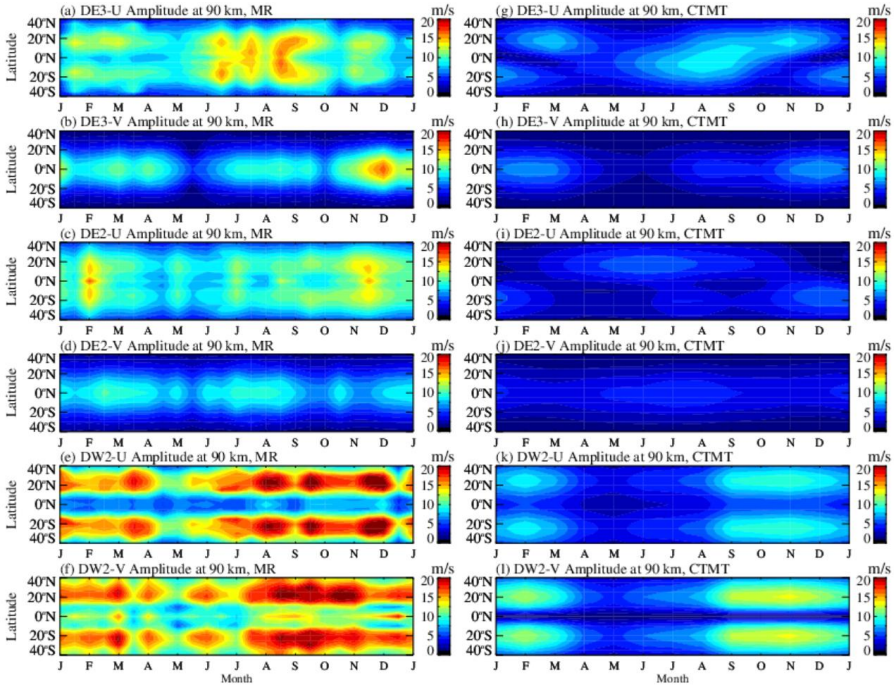


Figure 7: (a–f) The seasonal variation of DE3, DE2, and DW2 amplitudes in both zonal and meridional components at 90 km altitude in the latitude range of 40° S–40° N, decomposed by the hourly zonal and meridional wind over six meteor radars. (g–l) Same as (a–f), but from CTMT outputs.

Figure 7 presents the seasonal variations of DE3, DE2, and DW2 in different latitudes. Given that the latitudinal coverage of the observation stations ranges from 34.6°S to 25.6°N, Figure 7 presents only the results between 40°S and 40°N to avoid potential distortions at higher latitudes. In the meteor radar

https://doi.org/10.5194/egusphere-2026-6900
Preprint. Discussion started: 12 November 2026
© Author(s) 2026. CC BY 4.0 License.

observations, DE3-U is dominated by the symmetric Hough mode (-3, 3) during June–September, characterized by a maximum amplitude at the equator. In contrast, it is dominated by the antisymmetric mode (-3, 4) during January–April and November–December, with the minimum amplitude at the equator and the strongest amplitudes occurring near 20°S and 20°N. DE3-V and DE2-V are primarily controlled by the symmetric mode (-3, 3) and (-2, 2) throughout the year, respectively, while DE2-U exhibits a mixture of both symmetric mode (-2, 2) and antisymmetric mode (-2, 3). The latitudinal distributions of DW2-U and DW2-V are similar, both being dominated by the symmetric mode (2, 2), with maximum amplitudes occurring near 25°N and 25°S, and not zeros at Equator. Compared with the CTMT outputs, the hemispheric asymmetry in DE3-U and DE2-U is not reproduced in the observations. This may be attributable to the sparse latitudinal sampling of the station network, which allows at most two effective Hough modes to be resolved for each tidal component.

4.2 The impacts of SSW on nonmigrating tides

In addition to the seasonal variation, the variability of nonmigrating tides on shorter temporal scales can be investigated by the proposed method, as resolved from the calculated daily tidal amplitudes. During the observational time period 2005–2012, a significant atmospheric event, referred to as the stratospheric sudden warming (SSW) event, occurred in January 2006 (e.g., Hoffmann et al., 2007; Paulino et al., 2011; Sridharan et al., 2009). The SSW event is a dominant meteorological phenomenon occurring in the polar region of the winter hemisphere. In the winter polar region, enhanced tropospheric Rossby waves propagate upward into the stratosphere, depositing momentum and energy into the background atmosphere. This causes stratospheric temperatures to rise rapidly by up to 40 K within a few days (Andrews et al., 1987), weakening the intensity of the stratospheric westerly polar vortex and causing its structure to split and/or displacement, which is referred to as SSW events. A major SSW event is characterized by a rapid increase in stratospheric temperatures and a reversal of the zonal mean zonal wind at 60° latitude at 10 hPa; the significant feature of a minor event is that when the temperatures increase, the zonal mean zonal wind at 60° latitude at 10 hPa decrease but does not reverse (McInturff, 1978). Butler et al. (2015) suggested that the 2006 Northern Hemisphere SSW (NH-SSW) was classified as a major SSW event and identified the SSW central day (21 January 2006) as the date on which stratospheric temperatures reached their maximum. In addition, SSW events can also strongly affect vertical coupling across a large altitude range, from the ground surface up to the MLT/ionosphere (e.g., Matsuno, 1971; Pedatella and Forbes, 2010; Chau et al., 2012; Goncharenko et al., 2013; Li et al., 2021; Ye et al., 2021; Wang et al., 2022).

https://doi.org/10.5194/egusphere-2026-6900
Preprint. Discussion started: 12 November 2026
© Author(s) 2026. CC BY 4.0 License.

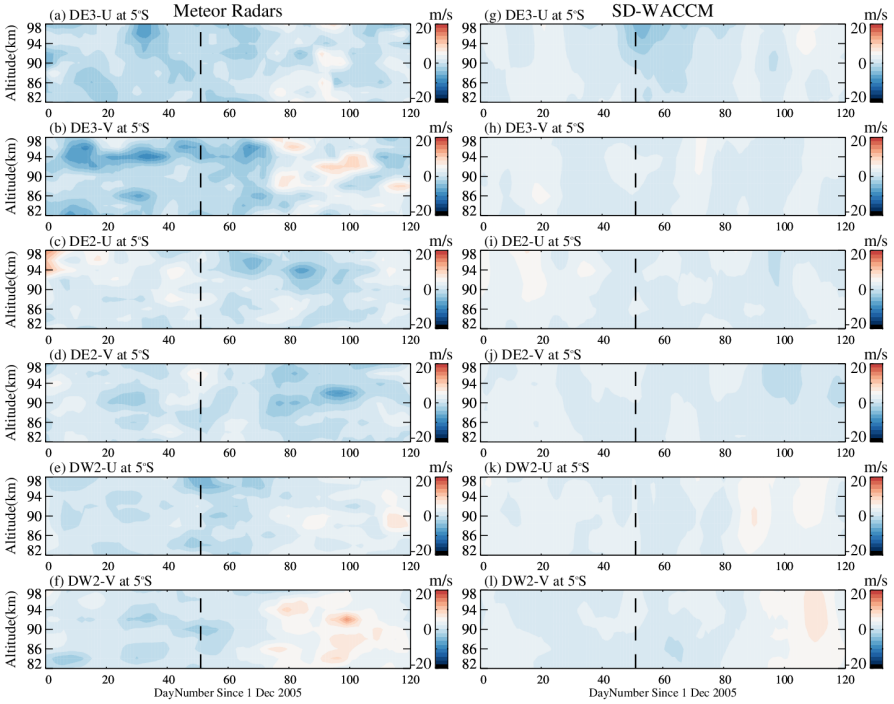


Figure 8: (a–f) The DE3, DE2, and DW2 amplitude anomalies in both zonal and meridional components at 5°S in the altitude range of 82–98 km, decomposed by the hourly zonal and meridional wind over six meteor radars. The anomalies are derived by removing the seasonal variation, annual oscillation, and semiannual oscillation. The black dashed lines indicate 21 January 2006. (g–l) Same as (a–f), but from WACCM simulations.

Figure 8 shows the anomalies of DE3, DE2, and DW2 amplitudes derived by removing the seasonal variation, annual oscillation, and semiannual oscillation, during the 2006 major SSW. In the observational results as shown in Figures 8a and 8b, the DE3 amplitudes at 5°S in both the zonal and meridional components are significantly suppressed (by ~-7 m/s for DE3-U and ~-6.6 m/s for DE3-V) from 25 December 2005 to 19 February 2006, corresponding to the period from 27 days before to 29 days after the SSW central day (21 January 2006). After 19 February 2006, the DE3-U amplitudes are slightly enhanced by ~4.2 m/s, and the DE3-V amplitudes are significantly enhanced by ~8.1 m/s above 86 km. However, in the WACCM simulation as shown in Figures 8g and 8h, the DE3 response to the SSW is presented only as a weakening of the DE3-U amplitude (by ~-8.2 m/s) from 6 January to 5 March 2006; during the time period from 1 December 2005 to 1 April 2006, both the positive perturbation in DE3-U and the perturbation in DE3-V are less than 2 m/s.

Figures 8c and 8d show the impact of 2006 SSW on DE2 tides in zonal and meridional components. The anomalies of DE2-U amplitudes are positive by ~3.4 m/s from 6 January 2006 to 16 January 2006 (corresponding to the period from 15 days to 5 days before the SSW central day), and negative by ~-9.4 m/s above 90 km from 25 January 2006 to 9 March 2006. The DE2-V amplitudes are slightly enhanced by ~4.2 m/s from 15 January 2006 to 24 January 2006 (corresponding to the period from 6 days before to 3 days after the SSW central day) and greatly weakened by ~-10.4 m/s from 9 February 2006 to 24

https://doi.org/10.5194/egusphere-2026-6900
Preprint. Discussion started: 12 November 2026
© Author(s) 2026. CC BY 4.0 License.

March 2006. In the WACCM simulations as shown in Figures 8i and 8j, both the DE2-U and DE2-V amplitudes are also reduced after the SSW central day, with the minimum of ~-2.8 m/s and ~-3.6 m/s, respectively. The anomalies of DE2-U amplitudes are positive with the maximum of ~4 m/s from 16 December to 11 January, slightly earlier than in the observations, whereas DE2-V amplitudes show no significant enhancement, with positive perturbations remaining below 2 m/s.

For the DW2 tidal components in the observational results (as shown in Figures 8e and 8f), The DW2-U amplitudes are significantly reduced by ~-8.1 m/s in the time period during from 10 January 2006 to 10 February 2006 and slightly enhanced by ~5.1 m/s after SSW central day from 12 February 2006 to 30 March 2006. The anomalies of DW2-V amplitudes are also characterized by a weakening around the SSW central day (from 22 December 2005 to 30 January 2006, corresponding to the period from 32 days before to 9 days after the SSW central day), with a minimum of ~-5.8 m/s, followed by an enhancement after the SSW central day (from 11 February 2006 to 21 March 2006), with a maximum of ~12.7 m/s. In WACCM simulations, the features of DW2 amplitudes in both zonal and meridional components are much similar to those in observational results.

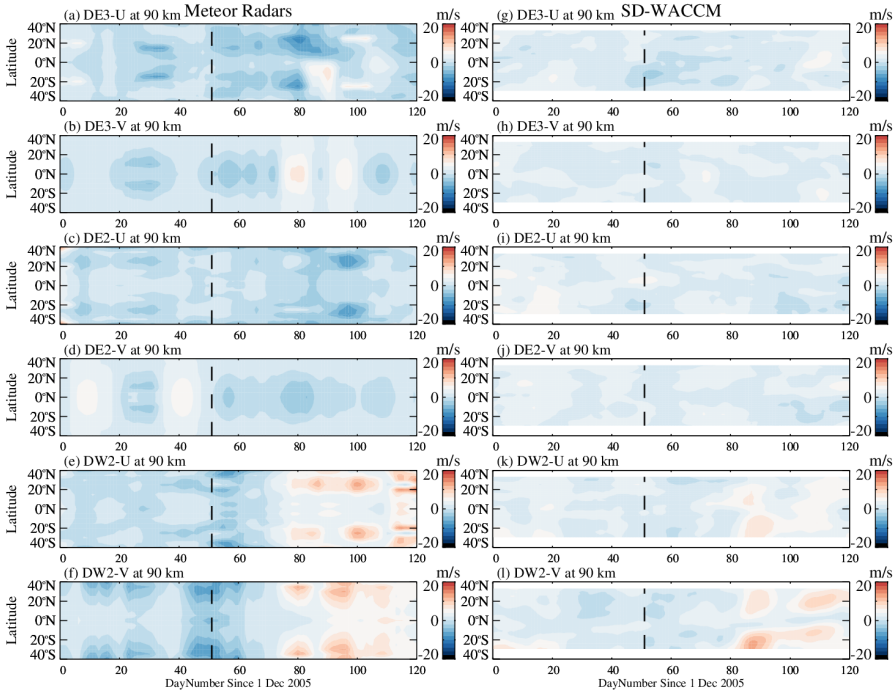


Figure 9: (a–f) The DE3, DE2, and DW2 amplitude anomalies in both zonal and meridional components at 90 km in the latitude range of 40°S–40°N, decomposed by the hourly zonal and meridional wind over six meteor radars. The black dashed lines indicate January 21, 2006. (g–l) Same as (a–f), but from WACCM simulations.

Also, the latitudinal variation features of different tidal components response to SSW are shown in Figure 9. In meteor radar observations, the strongest SSW responses are found in the antisymmetric Hough mode (-3, 4) and symmetric mode (-3, 3) for DE3-U, and in the symmetric Hough mode (-3, 3) for DE3-V. In the WACCM simulations, only the symmetric mode (-3, 3) shows a strong response to the SSW

https://doi.org/10.5194/egusphere-2026-6900
Preprint. Discussion started: 12 November 2026
© Author(s) 2026. CC BY 4.0 License.

for both zonal and meridional components. For DE2 tidal components, the observational results show that the first antisymmetric mode (-2, 3) and first symmetric mode (-2, 2) for DE2-U and first symmetric mode (-2, 2) for DE2-V show strong responses to the SSW, which is consistent with those in the WACCM simulations. During the 2006 SSW, the latitudinal variations of DW2 amplitudes in the observational results and WACCM simulations are highly consistent, in both zonal and meridional components, manifested as a strong response of the first symmetric Hough mode (2, 2).

These results that the proposed method successfully resolves not only the seasonal variation of nonmigrating tides but also their day-to-day variability during the 2006 SSW event. The significant response of DE3, DE2, and DW2 to the SSW provide strong evidence that the calculated daily tidal amplitudes capture dynamical coupling processes in the MLT region, via the amplitude anomalies and latitudinal structures of these tidal components.

The observational results indicate that the DE3 amplitudes, primarily reflected in the antisymmetric Hough mode (-3, 4) and symmetric mode (-3, 3) for DE3-U, as well as the symmetric Hough mode (-3, 3) for DE3-V, are suppressed from 25 December 2005 to 19 February 2006, spanning from 27 days before to 29 days after the SSW central day. This strong suppression is consistent with the known behavior of the DE3 tide during SSW events (Asamoah et al., 2025; Hu et al, 2026). The DE3 is primarily excited by latent heat release in the tropical troposphere and propagates upward to the middle and upper atmosphere (Oberheide et al., 2002; Miyoshi et al., 2017). During the 2006 SSW, the SSW-associated variations in the low-latitude zonal mean zonal wind and its meridional shear modify the propagation conditions for upward-propagating tides, leading to the suppression of DE3 in the MLT region (Hu et al., 2026). The delayed enhancement of DE3 after 19 February 2006 suggests a recovery of tidal propagation following the dissipation of the SSW. The slightly different response between DE3-U and DE3-V possibly reflects the different sensitivity of the two wind components to variations in the background wind structure and the Hough mode composition of the tide.

The DE2 response to the SSW is characterized by an enhancement of antisymmetric mode (-2, 3) and symmetric mode (-2, 2) before SSW and a delayed suppression after SSW. Although both DE3 and DE2 are eastward-propagating tides and are primarily excited by tropospheric latent heat release (Forbes et al., 2006; Miyoshi et al., 2017), the response of DE2 is greatly different from that of DE3. Based on the MERRA-2 reanalysis dataset, Asamoah et al. (2025) suggested that DE2 is more sensitive to secondary generation processes rather than being directly suppressed by background wind changes, possibly leading to the lagged response. In addition, enhanced planetary wave activity during SSWs provides favorable conditions for nonlinear interactions between planetary waves and tides, potentially leading to energy redistribution between DE2 and DE3. By using the linear Global Scale Wave Model (GSWM), Pedatella et al. (2012b) found that a 20-hour eastward propagating wave with eastward propagating zonal wavenumber 2 (20E2) can arise from the nonlinear interaction between DE3 and the quasi-6-day wave with westward propagating zonal wave number 1 (Q6W1). Given that the frequency and zonal wavenumber of 20E2 are nearly identical to those of DE2, the DE2 component obtained in our calculation may also incorporate a 20E2 contribution. Therefore, during the development of the SSW, DE3 is suppressed while DE2 is enhanced; after the dissipation of the SSW-induced planetary wave enhancement and background wind changes, DE3 is slightly enhanced whereas DE2 decreases.

The DW2 tidal component shows the strongest response among the three nonmigrating tides examined. The symmetric Hough mode (2, 2) of DW2 exhibits a suppression around the SSW central day, followed by a pronounced enhancement until March. The DW2 is known to be generated through the nonlinear

https://doi.org/10.5194/egusphere-2026-6900
Preprint. Discussion started: 12 November 2026
© Author(s) 2026. CC BY 4.0 License.

interaction between DW1 and the stationary planetary wave with westward propagating zonal wavenumber 1 (SPW1), and its strong response to the 2006 SSW reflects the intensified planetary wave activity in the winter stratosphere induced by the disruption of the stratospheric polar vortex. As the SSW develops, enhanced SPW1 activity generates DW2 through nonlinear interaction with DW1, while the variations in the zonal mean circulation filter the upward propagation of the generated DW2, leading to the DW2 response in the MLT region (Pancheva et al., 2009).

The nonmigrating tidal variability during the SSW also has important implications for the coupling between the middle atmosphere and ionosphere. The DE3 and DE2 tides, through its modulation of the E-region dynamo, generates the wave-4 and wave-3 structure in the equatorial vertical plasma drift and the associated wave-4 and wave-3 pattern in ionospheric parameters such as total electron content and electron density (Mukhtarov and Pancheva, 2011; Liao et al., 2026). The suppression of DE3 during the SSW would therefore be expected to weaken the wave-4 signature in the ionosphere, while the post-SSW enhancement of DE3 could lead to a strengthening of the wave-4 structure. Similarly, the DE2 and DW2 tides will contribute to the longitudinal variability of the ionospheric plasma density through their electrodynamic effects.

5 Conclusions

Horizontal winds observed by meteor radars in six longitudinal sectors are used to calculate nonmigrating tides. The neutral wind data were from 1 January 2005 to 31 December 2012 and derived from the meteor radars at Cariri (7.4° S, 36.5° W), Kototabang (0.2° S, 100.3° E), Ascension Island (7.9° S, 14.4° W), Darwin (12.3° S, 130.8° E), Buckland Park (34.6° S, 138.5° E), and Kunming (25.6°N, 103.8°E). According to the tidal fitting simulation based on WACCM winds, the migrating diurnal tides, DW1, and dominant nonmigrating diurnal components, including DE3, DE2, and DW2, could be extracted accurately by the six meteor radars.

The nonmigrating tidal amplitudes obtained from these six meteor radars exhibit significant seasonal and altitudinal variations, and their dominant Hough mode components are given. For all tidal components, the monthly mean amplitudes in the meridional components are larger than those in the zonal components. In the zonal component, the diurnal tidal amplitudes at 5°S in descending order are DW1, DE3, DE2, DW2, DW3, DS0, and DE1; in the meridional components, they are DE3, DW1, DW2, DE2, DS0, DE1, and DW3.

The climatology of the dominant nonmigrating tidal components, DE3, DE2, and DW2, in the observational results is consistent with the CTMT output, although their amplitudes are slightly larger than those from the CTMT output. The latitudinal variability of these nonmigrating tides at 5°S is also consistent with that of the CTMT, but the hemispheric asymmetries of DE3-U and DE2-U are not resolved. This may be attributable to the sparse latitudinal sampling of the station network, which allows at most two significant Hough modes to be resolved for each tidal component.

During the 2006 NH-SSW event, the amplitudes of DE3, DE2, and DW2 all exhibited significant variations. DE3 was suppressed during the development of the SSW and gradually recovered after the SSW dissipated; DE2 was enhanced during the development of the SSW and was rapidly suppressed after the SSW reached its maximum intensity; DW2 was suppressed around the SSW central day and greatly enhanced 20 days after the SSW central day. DE3 was suppressed because SSW-related changes in the background zonal wind and meridional wind shears disrupted the conditions for upward

https://doi.org/10.5194/egusphere-2026-6900
Preprint. Discussion started: 12 November 2026
© Author(s) 2026. CC BY 4.0 License.

propagation. The response of DE2 was nearly opposite to that of DE3, possibly related to nonlinear interactions with SSW-related planetary waves. DW2 formed through the nonlinear interaction between SPW1 and DW1 and was thus modulated by the SSW-related SPW1.

In this study, we report a method to decompose nonmigrating tidal winds by jointly analyzing six meteor radars over the low-latitude MLT region. The results presented in this study will provide an observational basis for further modeling studies of tidal dynamics impacts on the MLT region. In addition, our results will also provide a chance to investigate the coupling between the middle atmosphere and ionosphere through nonmigrating tides.

Data Availability. The Kototabang meteor radar data are available from http://database.rish.kyoto-u.ac.jp/arch/iugonet/mwr_ktb/index_mwr_ktb.html. The Ascension Island meteor radar data are available from https://data.ceda.ac.uk/badc/meteor-radars/data/ascension. The Cariri meteor radar data are available from https://doi.org/10.5281/zenodo.6575792 (Wang and Batista, 2022). The Darwin meteor radar data are available from https://doi.org/10.5281/zenodo.6575832 (Wang and Reid, 2022). The Kunming meteor radar data are available from https://doi.org/10.5281/zenodo.10829069 (Wang et al., 2024). The Buckland Park meteor radar data are available from https://doi.org/10.5281/zenodo.23921957 (Wang and Reid, 2026). The SD–WACCM dataset utilized in this study is available at https://doi.org/10.6084/m9.figshare.19777918 (Cen, 2022). The CTMT datasets are available from https://doi.org/10.5281/zenodo.5541913 (Oberheide, 2011).

Author contributions. Conceptualization, J.-Y.W., X.X.; data curation, X.X., Z.D., R.V., P.B., R.B., T.T. and N.M.; formal analysis, J.-Y.W. and W.Y.; funding acquisition, J.-Y.W., X.X, W.Y. and J.W.; investigation, J.-Y.W.; methodology, J.-Y.W., W.Y., X.X., I.R. and J.L.; project administration, X.X., W.Y. and X.D.; resources, X.X., T.C. and X.D.; software, J.-Y.W., J.-F.W., J.W. and J.Z.; supervision, X.X. and W.Y.; validation, X.X. and W.Y.; visualization, J.-Y.W.; writing—original draft preparation, J.-Y.W.; writing—review and editing, J.-Y.W., X.X, M.H. and W.Y.; All authors have read and agreed to the published version of the manuscript.

Competing interests. The authors declare that they have no conflict of interest.

Acknowledgments. This work is supported by National Natural Science Foundation of China (42504167 and 42574213), the National Key R&D Plan of China (Grant No. 2022YFF0503704), and the Project

https://doi.org/10.5194/egusphere-2026-6900
Preprint. Discussion started: 12 November 2026
© Author(s) 2026. CC BY 4.0 License.



Supported by the Specialized Research Fund for State Key Laboratory of Solar Activity and Space Weather. We acknowledge the use of data from the National Field Observation and Research Station (Yunnan Kunming) for Electromagnetic Environment. We acknowledge for the data resources from "National Space Science Data Center, National Science & Technology Infrastructure of China. (https://www.nssdc.ac.cn)".

References

Andrews, D., Holton, J., and Leovy, C.: Middle Atmosphere Dynamics, Academic Press, Inc., New York, 1987.

Asamoah, R. A., Tsidu, G. M., Garuma, G. F., and Amekudzi, L. K.: Observational Evidence of Distinct Excitation Pathways for Migrating and Non-Migrating Tides in the Mesosphere-Lower Thermosphere During the 2021 Sudden Stratospheric Warming. Atmosphere, 16(11), 1254. https://doi.org/10.3390/atmos16111254, 2025.

Baumgarten, K. and Stober, G.: On the evaluation of the phase relation between temperature and wind tides based on ground-based measurements and reanalysis data in the middle atmosphere, Ann. Geophys., 37, 581–602, https://doi.org/10.5194/angeo-37-581-2019, 2019.

Boyd, J. P.: The choice of spectral functions on a sphere for boundary and eigenvalue problems: A comparison of Chebyshev, Fourier and Associated Legendre expansions, Mon. Weather Rev., 106, 1184–1191, https://doi.org/ 10.1175/1520-0493(1978)106<1184:TCOSFO>2.0.CO;2, 1978.

Butler, A. H., Seidel, D. J., Hardiman, S. C., Butchart, N., Birner, T., and Match, A.: Defining sudden stratospheric warmings. Bulletin of the American Meteorological Society, 96(11), 1913-1928, https://doi.org/10.1175/BAMS-D-13-00173.1, 2015.

Cen, Y.: 1979–2014 SDWACCM data, figshare [data set], https://doi.org/10.6084/m9.figshare.19777918, 2022.

Chapman, S. and Lindzen, R.: Atmospheric tides – thermal and gravitational, D. Reidel Publishing Company, Dordrecht, the Netherlands, ISBN 978-94-010-3401-2, 1970.

Chau, J. L., Goncharenko, L. P., Fejer, B. G., and Liu, H.-L.: Equatorial and low latitude ionospheric effects during sudden stratospheric warming events, Space Sci. Rev., https://doi.org/10.1007/s11214-011-9797-5, 2012.

Dempsey, S. M., Hindley, N. P., Moffat-Griffin, T., Wright, C. J., Smith, A. K., Du, J., & Mitchell, N. J.: Winds and tides of the Antarctic mesosphere and lower thermosphere: One year of meteor-radar observations over Rothera (68°S, 68°W) and comparisons with WACCM and eCMAM. Journal of Atmospheric and Solar-Terrestrial Physics, 212, 105510. https://doi.org/10.1016/j.jastp.2020.105510, 2021.

Forbes, J. M., Zhang, X., Talaat, E. R., and Ward, W.: Nonmigrating diurnal tides in the thermosphere, J. Geophys. Res., 108, 1033, https://doi.org/10.1029/2002JA009262, A1, 2003.

Forbes, J. M., Russell, J., Miyahara, S., Zhang, X., Palo, S., Mlynczak, M., Hagan, M. E.: Troposphere–thermosphere tidal coupling as measured by the SABER instrument on TIMED during July–September 2002. J. Geophys. Res. Space Phys., 111, A10308, 2006.

https://doi.org/10.5194/egusphere-2026-6900
Preprint. Discussion started: 12 November 2026
© Author(s) 2026. CC BY 4.0 License.



Forbes, J. M., Zhang, X., Palo, S., Russell, J., Mertens, C. J., and Mlynczak, M.: Tidal variability in the ionospheric dynamo region. Journal of Geophysical Research, 113, A02310, https://doi.org/10.1029/2007JA012737, 2008.

Gauthier, A., Borries, C., Kozlovsky, A., Janches, D., Brown, P., Vida, D., Jacobi, C., Murphy, D., Tsutsumi, M., Gulbrandsen, N., Nozawa, S., Lester, M., Kero, J., Mitchell, N., Moffat-Griffin, T., and Stober, G.: TIMED Doppler Interferometer measurements of neutral winds at the mesosphere and lower thermosphere and comparison to meteor radar winds, Ann. Geophys., 43, 427–440, https://doi.org/10.5194/angeo-43-427-2025, 2025.

Goncharenko, L. P., Hsu, V. W., Brum, C. G. M., Zhang, S.-R., and Fentzke, J. T.: Wave signatures in the midlatitude ionosphere during a sudden stratospheric warming of January 2010, J. Geophys. Res. Space Physics, 118, 472–487, https://doi.org/10.1029/2012JA018251, 2013.

Griffith, M. J., Dempsey, S. M., Jackson, D. R., Moffat-Griffin, T., & Mitchell, N. J.: Winds and tides of the Extended Unified Model in the mesosphere and lower thermosphere validated with meteor radar observations. Annales Geophysicae, 39(3), 487–514. https://doi.org/10.5194/angeo-39-487-2021, 2021.

He, M., Liu, L., Wan, W., and Wei, Y.: Strong evidence for couplings between the ionospheric wave-4 structure and atmospheric tides, Geophysical Research Letters, 38, L14101, https://doi.org/10.1029/2011GL047855, 2011.

He, M., & Chau, J. L.: Mesospheric semidiurnal tides and near-12 h waves through jointly analyzing observations of five specular meteor radars from three longitudinal sectors at boreal midlatitudes. Atmospheric Chemistry and Physics, 19(9), 5993–6006. https://doi.org/10.5194/acp-19-5993-2019, 2019.

He, M., Chau, J. L., Stober, G., Li, G., Ning, B., & Hoffmann, P.: Relations between semidiurnal tidal variants through diagnosing the zonal wavenumber using a phase differencing technique based on two ground-based detectors. Journal of Geophysical Research: Atmospheres, 123, 4015–4026. https://doi.org/10.1002/2018JD028400, 2018.

Hocking, W. K., Fuller, B. and Vandepeer, B.: Real-time determination of meteor-related parameters utilizing modem digital technology, J. Atmos. Sol.-Terr. Phys., 63(2-3), 155-169, https://doi.org/10.1016/s1364-6826(00)00138-3, 2001.

Hoffmann, P., Singer, W., Keuer, D., Hocking, W.K., Kunze, M., Murayama, Y.: Latitudinal and longitudinal variability of mesospheric winds and temperatures during stratospheric warming events. Journal of Atmospheric and SolarTerrestrial Physics 69, 2355–2366, https://doi.org/10.1016/j.jastp.2007.06.010, 2007.

Holdsworth, D. A., Reid, I. M., and Cervera, M. A.: Buckland Park all-sky interferometric meteor radar, Radio Sci., 39(5), 12, https://doi.org/10.1029/2003rs003014, 2004.

Hu, P., Li, X., Ren, Z., Zou, J., and Cao, J.: Nonmigrating diurnal tide DE3 responses to the 2003/2004 sudden stratospheric warming. Journal of Geophysical Research: Space Physics, 131, e2026JA035052. https://doi.org/10.1029/2026JA035052, 2026.

Hurrell, J. W., Hack, J. J., Phillips, A. S., Caron, J., and Yin, J.: The dynamical simulation of the Community Atmosphere Model version 3 (CAM3), J. Climate, 19, 2162–2183, https://doi.org/10.1175/JCLI3762.1, 2006.

Isoda, F., Tsuda, T., Nakamura, T., Vincent, R. A., Reid, I. M., Achmad, E., Sadewo, A., and Nuryanto, A.: Intraseasonal oscillations of the zonal wind near the mesopause observed with medium-

https://doi.org/10.5194/egusphere-2026-6900
Preprint. Discussion started: 12 November 2026
© Author(s) 2026. CC BY 4.0 License.

675 frequency and meteor radars in the tropics, J. Geophys. Res., 109, D21108, https://doi.org/10.1029/2003JD003378, 2004.

Kumar, K. G., Singer, W., Oberheide, J., Grieger, N., Batista, P. P., Riggin, D. M., Schmidt, H., and Clemesha, B.R.: Diurnal tides at low latitudes: Radar, satellite, and model results. Journal of Atmospheric and Solar-Terrestrial Physics, 118, 96-105,
680 https://doi.org/10.1016/j.jastp.2013.07.005, 2014.

Lamarque, J.-F., Emmons, L. K., Hess, P. G., Kinnison, D. E., Tilmes, S., Vitt, F., Heald, C. L., Holland, E. A., Lauritzen, P. H., Neu, J., Orlando, J. J., Rasch, P. J., and Tyndall, G. K.: CAM-chem: description and evaluation of interactive atmospheric chemistry in the Community Earth System Model, Geosci. Model Dev., 5, 369–411, https://doi.org/10.5194/gmd-5-369-2012, 2012.

685 Li, N., Lei, J., Huang, F., Yi, W., Chen, J., Xue, X., et al.: Responses of the Ionosphere and Neutral Winds in the Mesosphere and Lower Thermosphere in the Asian-Australian Sector to the 2019 Southern Hemisphere Sudden Stratospheric Warming. Journal of Geophysical Research: Space Physics, 126(10), 1–15. https://doi.org/10.1029/2020JA028653, 2021.

Li, X., Wan, W., Ren, Z., Liu, L., and Ning, B.: The variability of nonmigrating tides detected from
690 TIMED/SABER observations, J. Geophys. Res. Space Physics, 120, 10, 793–10, 808, https://doi.org/10.1002/2015JA021577, 2015.

Li, X., Wan, W., Ren, Z., and Yu, Y.: The variability of SE2 tide extracted from TIMED/SABER observations, J. Geophys. Res. Space Physics, 122, 2136–2150, https://doi.org/10.1002/2016JA023435, 2017.

695 Li, X., Wan, W., Cao, J., Xue, X., & Ren, Z.: Hough Mode Decomposition of the DE3 tide extracted from TIMED observations. Journal of Atmospheric and Solar-Terrestrial Physics, 195, 105140. https://doi.org/10.1016/j.jastp.2019.105140, 2019a.

Li, X., Wan, W., Cao, J., & Ren, Z.: Meteorological scale correlation relationship of the ionospheric longitudinal structure wavenumber 4 and upper atmospheric daily DE3 tide. Journal of Geophysical
700 Research: Space Physics, 124, 2046–2057. https://doi.org/10.1029/2018JA026253, 2019b.

Li, X., Wan, W., Cao, J., Chen, T., &Ren, Z.: Hough mode decomposition of the SE2 tide extracted from TIMED observations. Journal of Geophysical Research: Space Physics, 125, e2020JA027898. https://doi.org/10.1029/2020JA027898, 2020.

Li, X., Ren, Z., Cao, J., Yu, Y., Wang, Y., & Zhou, X.: Comparative study of the variability of the non-
705 migrating tide DE3 using WACCM-X simulations and TIMED/SABER observations. Earth and Space Science, 9, e2021EA002117. https://doi.org/10.1029/2021EA002117, 2022.

Liao, L., Zhao, S., He, M., Cui, Y., and Li, J.: Atmospheric tides imprint a wavenumber-4 structure in topside ionospheric ELF wave intensity. Geophysical Research Letters, 53, e2026GL122255, https://doi.org/10.1029/2026GL122255, 2026.

710 Liu, G., Janches, D., Ma, J., Lieberman, R. S., Stober, G., Moffat-Griffin, T., et al.: Mesosphere and lower thermosphere winds and tidal variations during the 2019 Antarctic Sudden Stratospheric Warming. Journal of Geophysical Research: Space Physics, 127, e2021JA030177. https://doi.org/10.1029/2021JA030177, 2022.

Matsuno, T.: A Dynamical Model of the Stratospheric Sudden Warming. Journal of the Atmospheric
715 Sciences. https://doi.org/10.1175/1520-0469 (1971)028<1479, 1971.

McInturff, R. M.: Stratospheric warmings: Synoptic, dynamic and general-circulation aspects. NASA Reference Publ. NASA-RP-1017, 174 pp, [Available online at

https://doi.org/10.5194/egusphere-2026-6900
Preprint. Discussion started: 12 November 2026
© Author(s) 2026. CC BY 4.0 License.

http://ntrs.nasa.gov/archive/nasa/casi.ntrs.nasa.gov/19780010687.pdf.], 1978.

Miyoshi, Y., Pancheva, D., Mukhtarov, P., Jin, H., Fujiwara, H., and Shinagawa, H.: Excitation mechanism of non-migrating tides. J. Atmos. Sol.-Terr. Phys., 156, 24–36, https://doi.org/10.1016/j.jastp.2017.02.012, 2017.

Mukhtarov, P., and Pancheva, D.: Global ionospheric response to nonmigrating DE3 and DE2 tides forced from below, J. Geophys. Res., 116, A05323, https://doi.org/10.1029/2010JA016099, 2011.

Murphy, D. J.: Observations of a nonmigrating component of the semidiurnal tide over Antarctica. Journal of Geophysical Research, 108(D8), 4241. https://doi.org/10.1029/2002JD003077, 2003.

Murphy, D. J., Forbes, J. M., Walterscheid, R. L., Hagan, M. E., Avery, S. K., Aso, T., et al.: A climatology of tides in the Antarctic mesosphere and lower thermosphere. Journal of Geophysical Research, 111, D23104. https://doi.org/10.1029/2005JD006803, 2006.

Neale, R. B., Richter, J., Park, S., Lauritzen, P., Vavrus, S., Rasch, P., and Zhang, M.: The mean climate of the Community Atmosphere Model (CAM4) in forced SST and fully coupled experiments, J. Climate, 26, 5150–5168, https://doi.org/10.1175/JCLI-D-12-00236.1, 2013.

Nischal, N., Oberheide, J., Mlynczak, M. G., Marsh, D. R., & Gan, Q. (2019). Solar cycle variability of nonmigrating tides in the 5.3 and 15μm infrared cooling of the thermosphere (100–150 km) from SABER. Journal of Geophysical Research: Space Physics, 124, 2338–2356. https://doi.org/10.1029/2018JA026356, 2019.

Oberheide, J., Hagan, M. E., Roble, R. G., Offermann, D.: Sources of nonmigrating tides in the tropical middle atmosphere. J. Geophys. Res. Atmospheres, 107(D21), 4567, https://doi.org/10.1029/2002JD002220, 2002.

Oberheide, J., Forbes, J. M., Zhang, X., and Bruinsma, S. L.: Climatology of upward propagating diurnal and semidiurnal tides in the thermosphere. Journal of Geophysical Research, 116, A11306, https://doi.org/10.1029/2011JA016784, 2011.

Oberheide, J.: Climatological Tidal Model of the Thermosphere – CTMT, Zenodo [data set], https://doi.org/10.5281/zenodo.5541913, 2011.

Orszag, S. A.: Fourier Series on Spheres, Mon. Weather Rev., 102, 56–75, https://doi.org/10.1175/1520-0493(1974)102<0056:FSOS>2.0.CO;2, 1974.

Pancheva, D., Mukhtarov, P., and Andonov, B.: Nonmigrating tidal activity related to the sudden stratospheric warming in the Arctic winter of 2003/2004, Ann. Geophys., 27, 975–987, https://doi.org/10.5194/angeo-27-975-2009, 2009.

Paulino, A.R., Batista, P.P., Clemesha, R.: Lunar tides in the mesosphere and lower thermosphere over Cachoeira Paulista (22.71S; 45.01W). Journal of Atmospheric and Solar-Terrestrial Physics, in press, https://doi.org/10.1016/j.jastp.2011.04.018, 2011.

Paulino, A. R., Rodrigues, D. O., Paulino, I., Lima, L. M., Buriti, R. A., Batista, P. P., Ridley, A., and Wu, C.: Comparison of meteor radar and satellite winds in the Brazilian equatorial region, Ann. Geophys., 43, 183–191, https://doi.org/10.5194/angeo-43-183-2025, 2025.

Pedatella, N. M., and Forbes, J. M.: Evidence for stratosphere sudden warming ionosphere coupling due to vertically propagating tides, Geophys. Res. Lett., 37, L11104, https://doi.org/10.1029/2010GL043560, 2010.

Pedatella, N. M., Liu, H. L., and Richmond, A. D.: Atmospheric semidiurnal lunar tide climatology simulated by the Whole Atmosphere Community Climate Model, Journal of Geophysical Research: Space Physics, 117, A06327, https://doi.org/10.1029/2012ja017792, 2012a.

https://doi.org/10.5194/egusphere-2026-6900
Preprint. Discussion started: 12 November 2026
© Author(s) 2026. CC BY 4.0 License.

Pedatella, N. M., Liu, H.-L., and Hagan, M. E.: Day-to-day migrating and nonmigrating tidal variability due to the six-day planetary wave, J. Geophys. Res., 117, A06301, https://doi.org/10.1029/2012JA017581, 2012b.

Rebollo-Neira, L., and Lowe, D.: Optimized orthogonal matching pursuit approach, IEEE Signal Processing Letters, 9(4), 137-140, https://doi.org/10.1109/LSP.2002.1001652, 2002.

Smith, A. K., Pedatella, N. M., Marsh, D. R., and Matsuo, T.: On the Dynamical Control of the Mesosphere–Lower Thermosphere by the Lower and Middle Atmosphere, J. Atmos. Sci., 74(3), 933-947, https://doi.org/10.1175/jas-d-16-0226.1, 2017.

Sridharan, S., Sathishkumar, S., Gurubaran, S.: Variabilities of mesospheric tides and equatorial electrojet strength during major stratospheric warming events. Annales Geophysicae, 27, 4125–4130, https://doi.org/10.5194/angeo-27-4125-2009, 2009.

Stober, G., Baumgarten, K., McCormack, J. P., Brown, P., and Czarnecki, J.: Comparative study between ground-based observations and NAVGEM-HA analysis data in the mesosphere and lower thermosphere region, Atmos. Chem. Phys., 20, 11979–12010, https://doi.org/10.5194/acp-20-11979-2020, 2020.

Stober, G., Kuchar, A., Pokhotelov, D., Liu, H., Liu, H.-L., Schmidt, H., Jacobi, C., Baumgarten, K., Brown, P., Janches, D., Murphy, D., Kozlovsky, A., Lester, M., Belova, E., Kero, J., and Mitchell, N.: Interhemispheric differences of mesosphere–lower thermosphere winds and tides investigated from three whole-atmosphere models and meteor radar observations, Atmos. Chem. Phys., 21, 13855–13902, https://doi.org/10.5194/acp-21-13855-2021, 2021.

Truskowski, A. O., Forbes, J. M., Zhang, X., and Palo, S. E.: New perspectives on thermosphere tides: 1. Lower thermosphere spectra and seasonal-latitudinal structures. Earth, Planets and Space, 66, 136, https://doi.org/10.1186/s40623-014-0136-4, 2014.

Wang, H., Boyd, J. P., and Akmaev, R. A.: On computation of Hough functions, Geosci. Model Dev., 9, 1477–1488, https://doi.org/10.5194/gmd-9-1477-2016, 2016.

Wang, J., Yi, W., Wu, J., Chen, T., Xue, X., Zeng, J., et al.: Coordinated observations of migrating tides by multiple meteor radars in the equatorial mesosphere and lower thermosphere. Journal of Geophysical Research: Space Physics, 127, e2022JA030678. https://doi.org/10.1029/2022JA030678, 2022.

Wang, J., and Batista, P. P.: Zonal and meridional wind measured by meteor radar at Cariri, Zenodo [data set], https://doi.org/10.5281/zenodo.6575792, 2022.

Wang, J., and Reid, I. M.: Zonal and meridional wind measured by meteor radar at Darwin, Zenodo [data set], https://doi.org/10.5281/zenodo.6575832, 2022.

Wang, J., and Reid, I. M.: Zonal and meridional wind measured by Buckland Park meteor radar, Zenodo [data set], https://doi.org/10.5281/zenodo.23921957, 2026.

Wang, J., Li, N., and Ding, Z.: Zonal and meridional wind tides measured by Kunming meteor radar, Zenodo [data set], https://doi.org/10.5281/zenodo.10829069, 2024.

Wang, J., Yi, W., Xue, X., Wu, J., Ye, H., Chen, T., et al.: Impact of the Madden–Julian oscillation on mesospheric migrating diurnal tides observed by multiple equatorial meteor radars. Journal of Geophysical Research: Atmospheres, 130, e2025JD044411. https://doi.org/10.1029/2025JD044411, 2025.

Ward, W. E., Oberheide, J., Goncharenko, L. P., Nakamura, T., Hoffmann, P., Singer, W., Chang, L. C., Du, J., Wang, D.-Y., Batista, P., Clemesha, B., Manson, A. H., Riggin, D. M., She, C.-Y., Tsuda,

https://doi.org/10.5194/egusphere-2026-6900
Preprint. Discussion started: 12 November 2026
© Author(s) 2026. CC BY 4.0 License.



T., and Yuan, T.: On the consistency of model, ground-based, and satellite observations of tidal signatures: Initial results from the CAWSES tidal campaigns, J. Geophys. Res., 115, D07107, https://doi.org/10.1029/2009JD012593, 2010.

Wu, Q., Killeen, T. L., Ortland, D. A., Solomon, S. C., Gablehouse, R. D., Johnson, R. M., Skinner, W. R., Niciejewski, R. J., Franke, S. J.: TIMED Doppler Interferometer (TIDI) observations of migrating diurnal and semidiurnal tides. J. Atmos. Sol. Terr. Phys. 68 (3-5), 408–417, https://doi.org/10.1016/j.jastp.2005.02.031, 2006.

Wu, Q., Ortland, D. A., Killeen, T. L., Roble, R. G., Hagan, M. E., Liu, H.-L., Solomon, S. C., Xu, J., Skinner, W. R., and Niciejewski, R. J.: Global distribution and interannual variations of mesospheric and lower thermospheric neutral wind diurnal tide: 1. Migrating tide, J. Geophys. Res., 113, A05308, https://doi.org/10.1029/2007JA012542, 2008.

Wu, Q., Ortland, D. A., Solomon, S. C., Skinner, W. R., Niciejewski, R. J.: Global distribution, seasonal, and inter-annual variations of mesospheric semidiurnal tide observed by TIMED TIDI. J. Atmos. Sol. Terr. Phys. 73 (17), http://doi.org/10.1016/j.jastp.2011.08.007, 2011.

Xu, J., Smith, A. K., Liu, H.-L., Yuan, W., Wu, Q., Jiang, G., Mlynczak, M. G., Russell III, J. M., Franke, S. J.: Seasonal and quasi-biennial variations in the migrating diurnal tide observed by Thermosphere, Ionosphere, Mesosphere, Energetics and Dynamics (TIMED). J. Geophys. Res. 114, D13107, http://doi.org/10.1029/2008JD011298, 2009.

Xu, J., Smith, A. K., Jiang, G., Yuan, W., and Gao, H.: Features of the seasonal variation of the semidiurnal, terdiurnal and 6-h components of ozone heating evaluated from Aura/MLS observations, Ann. Geophys., 30, 259–281, https://doi.org/10.5194/angeo-30-259-2012, 2012.

Yang, C., Smith, A. K., Li, T., & Dou, X.: The effect of the Madden-Julian oscillation on the mesospheric migrating diurnal tide: A study using SD-WACCM. Geophysical Research Letters,45, 5105–5114. https://doi.org/10.1029/2018GL077956, 2018.

Ye, H., Xue, X., Yu, T., Sun, Y. Y., Yi, W., Long, C., et al.: Ionospheric F-Layer Scintillation Variabilities Over the American Sector During Sudden Stratospheric Warming Events. Space Weather, 19(8), 1–20. https://doi.org/10.1029/2020SW002703, 2021.

Yue, J., Xu, J., Chang, L., Wu, Q., Liu, H.-L., Lu, X., RussellI, J.: Global structure and seasonal variability of the migrating terdiurnal tide in the mesosphere and lower thermosphere. J. Atmos. Sol. Terr. Phys. 105–106, 191–198. https://doi.org/10.1016/j.jastp.2013.10.010, 2013.

Zhou, X., Chen, G., Yue, X., Zhang, R., & Yoshikawa, A.: Intraseasonal variability of the equatorial ionosphere responses to the Madden-Julian oscillation. Journal of Geophysical Research: Space Physics, 129(12), e2024JA033342. https://doi.org/10.1029/2024JA033342, 2024.

https://doi.org/10.5194/egusphere-2026-6900
Preprint. Discussion started: 12 November 2026
© Author(s) 2026. CC BY 4.0 License.

Appendix A: Figures A1

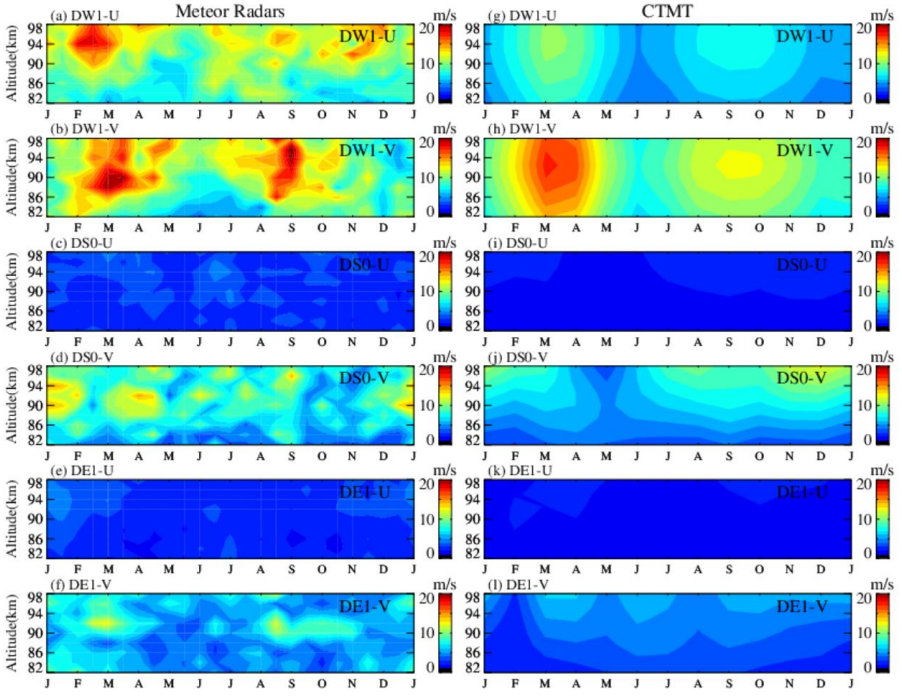


Figure A1: (a-f) The seasonal variation of DW1, DS0, and DE1 amplitudes in both zonal and meridional components at 5° S in the altitudinal range of 82-98 km, decomposed by the hourly zonal and meridional wind over six meteor radars. (g-l) Same as (a-f), but from CTMT outputs.